Self-Assembly Triangular and Square Rhenium(I) Tricarbonyl Complexes: A Comprehensive Study of Their Preparation, Electrochemistry, Photophysics, Photochemistry, and Host−Guest Properties

Shih-Sheng Sun and Alistair J. Lees*

Contribution from the Department of Chemistry, State University of New York at Binghamton, Binghamton, New York 13902-6016

Received May 15, 2000. Revised Manuscript Received June 30, 2000

Abstract: A series of self-assembly macrocyclic compounds featuring *fac*-$Re(CO)_3X$ (X = Cl or Br) as corners and linear bipyridyl bridging ligands have been prepared and characterized. Depending on the lengths as well as the bonding angles of the bridging ligands, the resulting geometries of these macrocyclic complexes are squares $\{[ClRe(CO)_3(\mu\text{-DPB})]_4$ (**3**) and $[ClRe(CO)_3(\mu\text{-AZP})]_4$ (**4**)}, triangles $\{[BrRe(CO)_3(\mu\text{-BPDB})]_3$ (**6**) and $[BrRe(CO)_3(\mu\text{-BPDDB})]_3$ (**7**)}, or a dimeric species $\{[ClRe(CO)_3(\mu\text{-BPET})]_2$ (**5**)}. A general mechanism for the self-assembly processes involving soluble intermediates is proposed. The photophysical properties of these macrocyclic compounds are dominated by the characteristics of the lowest excited states which vary from metal-to-ligand charge transfer (MLCT) to ligand-localized $\pi \rightarrow \pi^*$ or $n \rightarrow \pi^*$ transitions for the different molecules. Square **3** and triangles **6** and **7** are luminescent in room-temperature solution while square **4** and dimer **5** are nonemissive. An energy transfer mechanism from the MLCT excited state to the lowest nonemissive $n \rightarrow \pi^*$ excited state is attributed to the lack of emission in square **4**. The emission from square **3** is assigned to ^{3}MLCT character. In the cases of triangles **6** and **7**, emissions from the $^1\pi-\pi^*$ state were observed, as evidenced by their short lifetimes and structured emission bands. The large strain imposed on the triangular structures of **6** and **7** results in these molecules being photoactive. Photolysis of **6** or **7** at 313 nm is observed to break the triangular structure to form a polymeric structure. Square **4** exhibits reversible multielectron redox properties. Square **3** is also demonstrated to be a very effective host for nitro-substituted aromatic compounds.

Introduction

The degree of organization achieved by nature at the molecular level in many supramolecular assemblies formed from different molecular components has initiated the design of analogous synthetic assemblies during the last two decades.[1] In traditional studies of supramolecular self-assembly, hydrogen bonds are most frequently employed, as they are in all biological systems.[2] Relying on strong metal−ligand interactions, the design and study of well-arranged metal-containing macrocycles is one of the major current research areas in modern supramolecular chemistry.[3,4] Supramolecular species formed by self-assembly of transition metals with multidentate ligands represent an alternative to controlled processes involving biomimetic weak interactions (hydrogen bonding, $\pi-\pi$ stacking, van der Waals interactions, etc.).[5]

In the last 10 years, transition-metal-directed self-assembly has been used to construct many different supramolecular architectures such as squares,[6−10] helices,[11] boxes,[12] interlocked systems,[13,14] and many spectacular three-dimensional structures.[15] It has been well established that these macrocyclic compounds offer the feasibility of host−guest interactions and recognition phenomena based on Coulombic and/or hydrophobic bonding, where the binding affinity is highly dependent on the size of the cavity and the overall charge on the host molecules.[16]

(1) Lehn, J.-M. *Supramolecular Chemistry*; VCH Publishers: New York, 1995.
(2) Lawrence, D. S.; Jiang, T.; Levett, M. *Chem. Rev.* **1995**, *95*, 2229.
(3) Caulder, D. L.; Raymond, K. N. *J. Chem. Soc., Dalton Trans.* **1999**, 1185 and references therein.
(4) Leininger, S.; Olenyuk, B.; Stang, P. J. *Chem. Rev.* **2000**, *100*, 853 and references therein.
(5) Conn, M. M.; Rebek, J., Jr. *Chem. Rev.* **1997**, *97*, 1647.
(6) (a) Fujita, M.; Yazaki, J.; Ogura, K. *J. Am. Chem. Soc.* **1990**, *112*, 5645. (b) Fujita, M.; Yakazi, J.; Ogura, K. *Tetrahedron Lett.* **1991**, *32*, 5589. (c) Fujita, M.; Nagao, S.; Iida, M.; Ogura, K. *J. Am. Chem. Soc.* **1993**, *115*, 1574. (d) Fujita, M.; Sasaki, O.; Mitsuhashi, T.; Fujita, T.; Yazaki, J.; Yamaguchi, K.; Ogura, K. *Chem. Commun.* **1996**, 1535. (e) Fujita, M.; Aoyagi, M.; Ogura, K. *Inorg. Chim. Acta* **1996**, *246*, 53.
(7) (a) Stang, P. J.; Cao, D. H. *J. Am. Chem. Soc.* **1994**, *116*, 4981. (b) Stang, P. J.; Chen, K.; Arif, A. M. *J. Am. Chem. Soc.* **1995**, *117*, 6273. (c) Olenyuk, B.; Whiteford, J. A.; Stang, P. J. *J. Am. Chem. Soc.* **1996**, *118*, 8221. (d) Whiteford, J. A.; Lu, C. V.; Stang, P. J. *J. Am. Chem. Soc.* **1997**, *119*, 2524. (e) Stang, P. J.; Cao, D. H.; Chen, K.; Gray, G. M.; Muddiman, D. C.; Smith, R. D. *J. Am. Chem. Soc.* **1997**, *119*, 5163. (f) Manna, J.; Kuehl, C. J.; Whiteford, J. A.; Stang, P. J.; Muddiman, D. C.; Hofstadler, S. A.; Smith, R. D. *J. Am. Chem. Soc.* **1997**, *119*, 11611. (g) Muller, C.; Whiteford, J. A.; Stang, P. J. *J. Am. Chem. Soc.* **1998**, *120*, 9827.
(8) (a) Stricklen, P. M.; Volcko, E. J.; Verkade, J. G. *J. Am. Chem. Soc.* **1983**, *105*, 2494. (b) Jeong, K.-S.; Cho, Y. L.; Song, J. U.; Chang, H.-Y.; Choi, M.-G. *J. Am. Chem. Soc.* **1998**, *120*, 10982. (c) Cotton, F. A.; Daniels, L. M.; Lin, C.; Murillo, C. A. *Chem. Commun.* **1999**, 841. (d) Woessner, S. M.; Helms, J. B.; Houlis, J. F.; Sullivan, B. P. *Inorg. Chem.* **1999**, *38*, 4380. (e) Sun, S.-S.; Silva, A. S.; Brinn, I. M.; Lees, A. J. *Inorg. Chem.* **2000**, *39*, 1344.
(9) (a) Slone, R. V.; Yoon, D. I.; Calhoun, R. M.; Hupp, J. T. *J. Am. Chem. Soc.* **1995**, *117*, 11813. (b) Slone, R. V.; Hupp, J. T.; Stern, C. L.; Albrecht-Schmitt, T. E. *Inorg. Chem.* **1996**, *35*, 4096. (c) Slone, R. V.; Hupp, J. T. *Inorg. Chem.* **1997**, *36*, 5422. (d) Slone, R. V.; Benkstein, K. D.; Bélanger, S.; Hupp, J. T.; Guzei, I. A.; Rheingold, A. L. *Coord. Chem. Rev.* **1998**, *171*, 221. (e) Bélanger, S.; Hupp, J. T.; Stern, C. L.; Slone, R. V.; Watson, D. F.; Carrell, T. G. *J. Am. Chem. Soc.* **1999**, *121*, 557. (f) Bélanger, S.; Hupp, J. T. *Angew. Chem., Int. Ed.* **1999**, *38*, 2222.

10.1021/ja001677p CCC: $19.00
Published on Web 09/02/2000

The cavity inside the molecule also provides a potentially catalytic microreactor.[15b,17] Additionally, incorporation of photo- and/or redox-active centers into macrocyclic compounds is attractive in molecular sensing technology. This latter application provides an alternative to the detection of guest inclusion based on photoluminescence characteristics[9] or changes in redox potential values.[18] Another interesting feature of these multimetal chromophore supramolecules is their capability of harvesting light energy and undergoing a multielectron redox process.[19] These properties provide an opportunity for multielectron storage and subsequent multiple-electron transfer which is a necessary characteristic for energy conversion materials and/or electrocatalysts.[20]

Self-assembly squares have been the most well studied molecules among these supramolecular complexes. However, the majority of the molecular squares that have been prepared are based on the square-planar geometry of Pt(II) or Pd(II) complexes.[6,7,10] There are only a few examples of self-assembly molecular squares based on an octahedral geometry.[8,9] Also, in sharp contrast to the numerous examples of square structures reported, triangular complexes are much less common,[21,22] mainly due to the rarity of suitable building blocks with proper turning angles.[4] Nevertheless, triangular structures can be formed by carefully adjusting the experimental conditions and choosing appropriate bridging ligands.[6d,e,21h,22] We report herein the preparation and characterization of a series of *fac*-tricarbonyl rhenium(I)-based self-assembly macrocyclic compounds with various bridging ligands (Chart 1). It is demonstrated here that the geometry of these macrocyclic compounds can be varied among squares, triangles, or dimers by simply modifying the bridging ligand and that their resultant electrochemical, photophysical, and photochemical properties and binding capabilities toward guest molecules are very different.

Chart 1

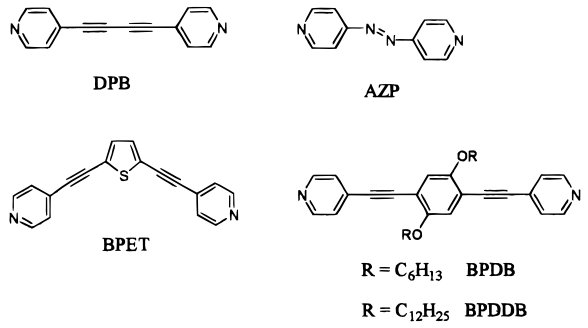

Experimental Section

Materials and General Procedures. Except for those mentioned below, all chemicals were commercially available and used without further purification. All reactions and manipulations were carried out under N_2 or Ar with the use of standard inert-atmosphere and Schlenk techniques. Solvents used for synthesis were dried by standard procedures and stored under N_2.[23] Solvents used in luminescent and electrochemical studies were spectroscopic and anhydrous grade, respectively. The 4,4′-dipyridylbutadiyne (DPB),[24] 4,4′-azopyridine (AZP),[25] 1,4-bis(4′-pyridylethynyl)-2,5-dihexyloxybenzene (BPDB),[22] and 2,5-bis(4-pyridylethynyl)thiophene (BPET)[26] ligands were prepared according to published methods. The 1,4-bis(4′-pyridylethynyl)-2,5-didodecyloxybenzene (BPDDB, **2**) ligand was synthesized by following the same procedure as reported for BPDB (**1**).[22] Tetrabutylammonium perchlorate (TBAP) used as supporting electrolyte in cyclic voltammetry was dried in a vacuum oven at 100 °C for 24 h prior to use. Nitrogen used for the synthesis and purging experiments was dried and deoxygenated according to a previously reported method.[27]

Film Preparation. Thin films were prepared by first dissolving the sample in THF. These solutions were then filtered to remove any undissolved particles present and then spin cast on clean borosilicate glass slides. The "wet" film was subsequently dried under vacuum overnight before acquiring the luminescence measurements.

Equipment and Procedures. NMR spectra were obtained using a Brücker AM 360 spectrometer. Infrared spectra were measured on a Nicolet 20SXC Fourier Transform infrared spectrophotometer. Fast atom bombardment (FAB) mass spectra were obtained on a Finnigan Mat 95 mass spectrometer. Elemental analysis was performed by Oneida Research Service, Whitesboro, New York. Absorption spectra were

(10) (a) Rauter, H.; Hillgeris, E. C.; Erxleben, A.; Lipper, B. *J. Am. Chem. Soc.* **1994**, *116*, 616. (b) Drain, C. M.; Lehn, J.-M. *J. Chem. Soc., Chem. Commun.* **1994**, 2313. (c) Zhang, Y.; Wang, S.; Enright, G. D.; Breeze, S. R. *J. Am. Chem. Soc.* **1998**, *120*, 9398. (d) Onitsuka, K.; Yamamoto, S.; Takahashi, S. *Angew. Chem., Int. Ed. Engl.* **1999**, *38*, 174.

(11) Constable, E. C. *Comprehensive Supramolecular Chemistry*; Atwood, J. L., Davies, J. E. D., MacNicol, D. D., Vogtle, F., Lehn, J.-M., Eds.; Pergamon: Oxford, 1996; Vol. 9, Chapter 6, pp 213−252 and references therein.

(12) Baxter, P. N. W.; Lehn, J.-M.; Kneisel, B. O.; Fenske, D. *Chem. Commun.* **1997**, 2231.

(13) (a) Fujita, M.; Ibukuro, F.; Hagihara, H.; Ogura, K. *Nature* **1994**, *367*, 720. (b) Fujita, M.; Fujita, N.; Ogura, K.; Yamaguchi, K. *Nature* **1999**, *400*, 52. (c) Fujita, M. *Acc. Chem. Res.* **1999**, *32*, 53 and references therein.

(14) (a) Sauvage, J.-P.; Dietrich-Buchecker, C. O.; Chambron, J.-C. In *Comprehensive Supramolecular Chemistry*; Lehn, J.-M., Ed.; Pergamon Press: Oxford, 1995; Vol. 9, Chapter 2 and references therein. (b) Stoddart, J. F.; Raymo, F.; Amabillino, D. B. In *Comprehensive Supramolecular Chemistry*; Lehn, J.-M., Ed.; Pergamon Press: Oxford, 1995; Vol. 9, Chapter 3 and references therein.

(15) (a) Fujita, M.; Ogura, D.; Miyazawa, M.; Oka, H.; Yamaguchi, K.; Ogura, K. *Nature* **1995**, *378*, 469. (b) Kang, J.; Rebek, J., Jr. *Nature* **1997**, *385*, 50. (c) Takeda, N.; Umemoto, K.; Yamaguchi, K.; Fujita, M. *Nature* **1999**, *398*, 794. (d) Olenyuk, B.; Whiteford, J. A.; Fechtenkotter, A.; Stang, P. J. *Nature* **1999**, *398*, 796. (e) Aoyagi, M.; Biradha, K.; Fujita, M. *J. Am. Chem. Soc.* **1999**, *121*, 7457. (f) Olenyuk, B.; Levin, M. D.; Whiteford, J. A.; Shield, J. E.; Stang, P. J. *J. Am. Chem. Soc.* **1999**, *121*, 10434.

(16) Atwood, J. L., Ed. *Inclusion Phenomena and Molecular Recognition*; Plenum Press: New York, 1990.

(17) Fujita, M.; Kwon, Y. J.; Washizu, S.; Ogura, K. *J. Am. Chem. Soc.* **1994**, *116*, 1151.

(18) (a) Beer, P. D.; Szemes, F.; Balzani, V.; Sala, C. M.; Drew, M. G. B.; Dent, S. W.; Maestri, M. *J. Am. Chem. Soc.* **1997**, *119*, 11864. (b) Beer, P. D.; Gale, P. A.; Chen, G. Z. *J. Chem. Soc., Dalton Trans.* **1999**, 1897 and references therein.

(19) (a) Lees, A. J. *Chem. Rev.* **1987**, *87*, 711. (b) Gamelin, D. R.; George, M. W.; Glynn, P.; Grevels, F.-W.; Johnson, F. P. A.; Klotzbücher, W.; Morrison, S. L.; Russell, G.; Schaffner, K.; Turner, J. J. *Inorg. Chem.* **1994**, *33*, 3246. (c) Balzani, V.; Juris, A.; Venturi, M.; Campagna S.; Serroni, S. *Chem. Rev.* **1996**, *96*, 759.

(20) (a) Astruc, D. *Electron Transfer and Radical Processes in Transition-Metal Chemistry*; VCH Publishers: New York, 1995. (b) Brudvig, G. W.; Thorp, H. H.; Crabtree, R. H. *Acc. Chem. Res.* **1991**, *24*, 311.

(21) Nevertheless, the appearances of triangular structures in the literature have rapidly increased in recent years. Some selective examples include: (a) Ruttimann, S.; Bernardinelli, G.; Williams, A. F. *Angew. Chem., Int. Ed. Engl.* **1993**, *32*, 392. (b) Barbera, J.; Elduque, A.; Gimenez, R.; Oro, L. A.; Serrano, J. L. *Angew. Chem., Int. Ed. Engl.* **1996**, *35*, 2832. (c) Lee, S. B.; Hwang, S.; Chung, D. S.; Yun, H.; Hong, J.-I. *Tetrahedron Lett.* **1998**, *39*, 873. (d) Hall, J. R.; Loeb, S. J.; Shimizu, G. K. H.; Yap, G. P. A. *Angew. Chem., Int. Ed. Engl.* **1998**, *37*, 121. (e) McQuillan, F. S.; Berridge, T. E.; Chen, H.; Hamor, T. A.; Jones, C. J. *Inorg. Chem.* **1998**, *37*, 4959. (f) Thompson, A.; Rettig, S. J.; Dolphin, D. *Chem. Commun.* **1999**, 631. (g) Lai, S.-W.; Chan, M. C.-W.; Peng, S.-M.; Che, C.-M. *Angew. Chem., Int. Ed. Engl.* **1999**, *38*, 669. (h) Cotton, F. A.; Daniels, L. M.; Lin, C.; Murillo, C. A. *J. Am. Chem. Soc.* **1999**, *121*, 4538. (i) Habereder, T.; Warchhold, M.; Nöth, H.; Severin, K. *Angew. Chem., Int. Ed. Engl.* **1999**, *38*, 3225. (j) Schnebeck, R.-D.; Freisinger, E.; Glahé, F.; Lippert, B. *J. Am. Chem. Soc.* **2000**, *122*, 1381.

(22) Sun, S.-S.; Lees, A. J. *Inorg. Chem.* **1999**, *38*, 4181.

(23) Perrin, D. D.; Armarego, W. L. F.; Perri, D. R., Eds. *Purification of Laboratory Chemicals*, 2nd ed.; Pergamon Press: Oxford, U.K., 1980.

(24) Ciana, L. D.; Haim, A. *J. Heterocycl. Chem.* **1984**, *21*, 607.

(25) Launay, J.-P.; Tourrel-Pagis, M.; Lipskier, J.-F.; Marvaud, V.; Joachim, C. *Inorg. Chem.* **1991**, *30*, 1033.

(26) (a) Neenan, T. X.; Whitesides, G. M. *J. Org. Chem.* **1988**, *53*, 2489. (b) Wu, I.-Y.; Lin, J. T.; Luo, J.; Li, C.-S.; Tsai, C.; Wen, Y. S.; Hsu, C.-C.; Yeh, F.-F.; Liou, S. *Organometallics* **1998**, *17*, 2188.

(27) Schadt, M. J.; Lees, A. J. *Inorg. Chem.* **1986**, *25*, 672.

obtained using a HP 8450A diode array spectrophotometer interfaced to an IBM computer.

Emission and excitation spectra were recorded in deoxygenated solvent solution at 293 K with an SLM 48000S lifetime fluorescence spectrophotometer equipped with a red-sensitive Hamamatsu R928 photomultiplier tube. The emission spectra were collected on samples with OD $\sim$ 0.1 at the excitation wavelength. Low-temperature emission spectra were performed using an Oxford Instruments DN1740K liquid-nitrogen cryostat equipped with an external Oxford Instruments Model 3120 temperature controller. In all emission experiments, the sample solutions were filtered through 0.22-μm Millipore filters prior to measurement. UV−visible spectra were checked before and after irradiation to monitor possible sample degradation. Emission maxima were reproducible to within 2 nm. Luminescence quantum yields (Φ_{em}) for metal complexes and organic ligands were calculated relative to $[Ru(bpy)_3]^{2+}$ in air-equilibrated aqueous solution ($\Phi_{em} = 0.028$) and perylene in deoxygenated EtOH solution ($\Phi_{em} = 0.89$), respectively.[28] Luminescence quantum yields were taken as the average of three separate determinations and were reproducible to within 10%.

Film luminescence measurements were obtained by placing the sample film at a 22.5° angle to the incident beam. The film glass slide and nitro-substituted aromatic compound were placed in a sealed 50-mL vial separated by cotton. The luminescence spectra were obtained before and after exposing the films to the vapor of nitro-substituted aromatic compounds for 3 mins.

Room-temperature luminescence lifetimes were recorded on a SLM 48000S phase-modulation lifetime fluorescence spectrophotometer. The excitation light passed through a monochromator and was then intensity modulated at a different frequency by a Debye-Sears ultrasonic modulator. The sample and reference solutions were placed in a two-chamber turret. The emission intensities of each at the observation wavelength were approximately balanced by neutral density filters. The phase shift and modulation of each sample was measured alternately 25 times. The results were averaged and analyzed by an interfaced IBM computer. For a single-exponential decay, the phase (ϕ) and modulation (m) are related to the lifetime (τ) according to the following equations: $\tan \phi\omega = \omega\tau$ and $m\omega = (1 + \omega^2\tau^2)^{-1/2}$, where ω is the angular modulation frequency (2π times the modulation frequency in hertz). The errors for the fitted lifetimes are estimated to be within 10%.

Low-temperature luminescence lifetimes and solution lifetimes longer than 50 ns were obtained using a Molectron Pulsed Nd:YAG laser (λ_{ex} = 355 nm) system as the excitation source and a Tektronix 7612A digitizer was used for decay data acquisition. The excited-state decay was then fitted by a least-squares method according to the equation $I(t) = I_0 \exp(-t/\tau)$, where $I(t)$ is the emission intensity at time t after the laser pulse and I_0 is the initial intensity at $t = 0$. Single exponential decays were observed in each case and the obtained lifetimes were found to be reproducible to within ±5%.

Photolysis experiments were carried out with a 200-W medium-pressure Hg arc lamp with Ealing Corp. interference filters (10-nm band-pass) to isolate the excitation wavelength. Sample solutions prepared in 1,2-dichloroethane (1,2-DCE) were filtered through 0.22-μm Millipore filters immediately before use and then deoxygenated prior to photolysis. Throughout photolysis the solutions were rapidly stirred to ensure sample homogeneity and a uniform optical density in the light path. All reactions were also performed in the dark to assess the extent of thermal processes, which were found to be negligible under our experimental conditions.

Molecular weights of photolysis products were estimated via gel permeation chromatography (GPC). A Waters 510 dual reciprocating piston pump with 100-μL heads delivered the deoxygenated toluene mobile phase at a flow rate of 1.00 mL/min. The pump was controlled by a Waters Pump Control Module run by Waters Millennium chromatography software. All samples were prepared in toluene. Data points were collected every 0.25 s, and molecular weights were calculated relative to polystyrene standards using Wyatt Technology Corporation's ASTRA chromatography software, version 4.20, on a PC.

(28) (a) Nakamaru, K. *Bull. Chem. Soc. Jpn.* **1982**, *55*, 2697. (b) Walters, K. A.; Ley, K. D.; Schanze, K. S. *Chem. Commun.* **1998**, 1115.

Electrochemical measurements were recorded on a Princeton Applied Research Model 263A potentiostat (EG&G instruments). The electrochemical cell consisted of a platinum working electrode, a platinum wire counter electrode, and a $Ag/AgNO_3$ (0.1 M in CH_3CN solution) reference electrode. Cyclic voltammograms were obtained in deoxygenated anhydrous solvent with the electroactive material (1.0×10^{-3} M) and 0.1 M TBAP as supporting electrolyte. Ferrocene (Fc) was used as an internal standard for both potential calibration and reversibility criteria. All potentials for the complexes in the study are reported relative to Fc/Fc^+. The scan rate was 250 mV/s, unless otherwise noted, and the measurements were uncorrected for liquid-junction potentials.

General Procedure for Synthesis of the Square Complexes, $[XRe(CO)_3(\mu\text{-}L)]_4$. To a flask (250 mL) containing a 1:1 molar ratio of $XRe(CO)_5$ and bridging ligand (L) was added 80 mL of toluene/THF (1:1 v/v) and the solution was heated at 70 °C for 48 h. The solution volume was then reduced to half under reduced pressure. Subsequently, the precipitate was collected and dried in vacuo to afford an analytical pure product with a yield typically higher than 90%.

Square 3 (X = Cl, L = DPB): IR (DMF, υ_{CO}, cm^{-1}) 2021, 1928, 1892. ^1H NMR (DMSO-d_6) 8.73 (d, $^3J_{H-H}$ = 6.5 Hz, 16 H, PyH_α), 7.77 (d, $^3J_{H-H}$ = 6.5 Hz, 16 H, PyH_β). ^{13}C NMR (acetone-d_6) 196.5, 192.1, 155.7, 155.6, 132.2, 129.4, 81.4, 79.9. MS (FAB, *m*-NBA as matrix) *m*/*z* 2002.4 (M − Cl^-) (calculated *m*/*z* 2003 for M − Cl^-). Anal. Calcd for $Cl_4C_{68}H_{32}N_8O_{12}Re_4$: C, 40.00; H, 1.58; N, 5.49. Found: C, 39.86; H, 1.44; N, 5.61.

Square 4 (X = Cl, L = AZP): IR (DMF, υ_{CO}, cm^{-1}) 2023, 1922, 1895. ^1H NMR (DMSO-d_6) 9.01 (d, $^3J_{H-H}$ = 6.0 Hz, 16 H, PyH_α), 7.97 (d, $^3J_{H-H}$ = 6.1 Hz, 16 H, PyH_β). The solubility of **4** is too low in organic solvent to obtain the ^{13}C spectrum. MS (FAB) *m*/*z* 1961.1 (M + H^+) (calculated *m*/*z* 1960.9 for M + H^+). Anal. Calcd for $Cl_4C_{52}H_{32}N_{16}O_{12}Re_4$: C, 31.84; H, 1.65; N, 11.43. Found: C, 31.49; H, 1.78; N, 11.23.

$[ClRe(CO)_3(\mu\text{-}BPET)]_2$ (5): The procedure for preparing the dimer **5** is similar to the preparation of the square complexes. The yellow solid collected from the toluene/THF mixture was subjected to column chromatography on silica gel eluting with CH_2Cl_2/THF (4:1 v/v). The second major yellow band was collected and the volume was reduced to $\sim$5 mL. This solution was slowly added to a rapidly stirring cold pentane solution (250 mL). The resulting fine yellow powder was collected and dried in vacuo. Yield 71%. IR (CH_2Cl_2, υ_{CO}, cm^{-1}) 2027, 1926, 1891. ^1H NMR (acetone-d_6): 8.83 (d, $^3J_{H-H}$ = 6.8 Hz, PyH_α), 7.65 (d, $^3J_{H-H}$ = 6.8 Hz, PyH_β), 7.57 (s, $H_{thiophene}$). ^{13}C NMR (acetone-d_6) 197.1, 193.0, 154.8, 136.1, 134.0, 128.2, 125.5, 92.2, 90.3. MS (FAB, *m*-NBA as matrix) *m*/*z* 1148.9 (M − Cl^-) (calculated *m*/*z* 1149 for M − Cl^-). Anal. Calcd for $Cl_2C_{42}H_{20}N_4O_6S_2Re_2$: C, 42.57; H, 1.70; N, 4.73. Found: C, 42.94; H, 1.66; N, 4.15. Alternatively, **5** can be prepared as a single product with 86% isolated yield by prolonging the reaction period to 1 week.

General Procedure for Synthesis of the Triangular Complexes, $[BrRe(CO)_3(\mu\text{-}L)]_3$. To a flask (250 mL) containing 1:1 molar ratio of $BrRe(CO)_5$ and bridging ligand (L) was added benzene (80 mL) and the resulting solution was heated at 70 °C for 48 h. The solvent was reduced to half and hexane (100 mL) was added to force further precipitation. The precipitate was collected and dried in vacuo to afford an analytically pure product with a yield typically higher than 90%.

Triangle 6 (L = BPDB): IR (CH_2Cl_2, υ_{CO}, cm^{-1}) 2027, 1928, 1893. ^1H NMR ($CDCl_3$) 8.77 (d, J_{H-H} = 6.6 Hz, 12H, PyH_α), 7.34 (d, $^3J_{H-H}$ = 6.5 Hz, 12 H, PyH_β), 7.00 (s, 6 H, Ph), 4.01 (t, $^3J_{H-H}$ = 6.5 Hz, 12 H, $-OCH_2C_5H_{11}$), 1.81 (t, $^3J_{H-H}$ = 6.6 Hz, 12 H, $-OCH_2CH_2C_4H_9$), 1.50−1.33 (m, 36 H, $-OC_2H_4C_3H_6CH_3$), 0.87 (m, 18 H, $-OC_5H_{10}CH_3$). ^{13}C NMR ($CDCl_3$) 195.1, 154.4, 154.3, 134.3, 127.5, 117.0, 113.9, 95.1, 91.7, 69.8, 31.7, 29.3, 25.8, 22.8, 14.2. MS (FAB, *m*-NBA as matrix) *m*/*z* 2494.2 (M + H^+) (calculated *m*/*z* 2493), 2412.1 (M − Br^-) (calculated *m*/*z* 2412). Anal. Calcd for $Br_3C_{105}H_{108}N_6O_{15}Re_3$: C, 50.59; H, 4.37; N, 3.37. Found: C, 50.11; H, 4.79; N, 3.03.

Triangle 7 (L = BPDDB): IR (CH_2Cl_2, υ_{CO}, cm^{-1}) 2027, 1926, 1893. ^1H NMR ($CDCl_3$) 8.81 (d, $^3J_{H-H}$ = 6.2 Hz, 12 H, PyH_α), 7.37 (d, $^3J_{H-H}$ = 6.4 Hz, 12 H, PyH_β), 7.03 (s, 6 H, Ph), 4.03 (t, $^3J_{H-H}$ = 6.4 Hz, 12 H, $-OCH_2C_{11}H_{23}$), 1.85 (q, $^3J_{H-H}$ = 7.4 Hz, 12 H, $-OCH_2CH_2C_{10}H_{21}$), 1.51 (q, $^3J_{H-H}$ = 7.0 Hz, 12 H, $-OC_2H_4CH_2C_9H_{19}$), 1.25 (m, 96 H, $-OC_3H_6C_8H_{16}CH_3$), 0.87 (t, $^3J_{H-H}$ = 6.8 Hz, 18 H,

Scheme 1

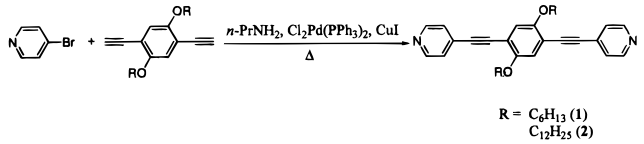

$-OC_{11}H_{22}CH_3$). ^{13}C NMR ($CDCl_3$) 195.0, 192.0, 154.4, 154.3, 134.3, 127.5, 117.0, 113.9, 95.1, 91.7, 69.8, 32.1, 29.8, 29.54, 29.49, 29.4, 26.1, 22.9, 14.3. MS (FAB, *m*-NBA as matrix) *m*/*z* 2997.1 ($M + H^+$) (calculated *m*/*z* 2996). Anal. Calcd for $Br_3C_{141}H_{180}N_6O_{15}Re_3$: C, 56.50; H, 6.05; N, 2.80. Found: C, 56.29; H, 5.75; N, 2.78.

General Procedure for Synthesis of $BrRe(CO)_3(L)_2$. To a two-neck flask (100 mL) containing 101.5 mg (0.25 mmol) of $BrRe(CO)_5$ and L (1 mmol) was added nitrogen-degassed isooctane (30 mL) and the resulting mixture was refluxed under nitrogen for 6 h. The precipitate was collected on the frit while the solution was still hot and then washed with hot isooctane (20 mL × 5) and dried in vacuo. Typically, no further purification is needed.

Corner 8 {*fac*-$BrRe(CO)_3(DPB)_2$}: Yield 92%. IR (υ_{CO}, cm^{-1}, CH_2Cl_2) 2028, 1929, 1894. ^1H NMR (DMSO-d_6) 8.77 (d, 4H, H_αPy-Re, $^3J_{H-H}$ = 6.5 Hz), 8.68 (d, 4 H, H_αPy, $^3J_{H-H}$ = 5.8 Hz), 7.76 (d, 4 H, H_β-Re, $^3J_{H-H}$ = 6.6 Hz), 7.62 (d, 4 H, H_βPy, $^3J_{H-H}$ = 5.8 Hz). ^{13}C NMR (DMSO-d_6) 195.6, 191.0, 154.4, 150.1, 130.9, 128.6, 127.5, 126.1, 82.4, 79.6, 79.2, 75.8. Anal. Calcd for $C_{31}H_{16}N_4BrO_3Re$: C, 49.08; H, 2.13; N, 7.39. Found: C, 49.23; H, 2.21; N, 7.29.

Corner 9 {*fac*-$BrRe(CO)_3(AZP)_2$}: Yield 98%. IR (υ_{CO}, cm^{-1}, CH_2Cl_2) 2028, 1930, 1895. ^1H NMR (acetone-d_6): 9.21 (d, 4H, H_αPy-Re, $^3J_{H-H}$ = 6.8 Hz), 8.90 (d, 4 H, H_αPy, $^3J_{H-H}$ = 6.3 Hz), 7.98 (d, 4 H, H_β-Re, $^3J_{H-H}$ = 6.8 Hz), 7.83 (d, 4 H, H_βPy, $^3J_{H-H}$ = 6.2 Hz). ^{13}C NMR (DMSO-d_6) 195.7, 191.2, 156.9, 156.6, 156.1, 151.8, 118.6, 116.0 Anal. Calcd for $C_{23}H_{16}N_8BrO_3Re$: C, 38.43; H, 2.23; N, 15.60. Found: C, 38.26; H, 2.09; N, 15.74.

Results and Discussion

Synthesis, Characterization, and General Properties. The bridging ligands DPB, AZP, and BPET were synthesized by published methods. Ligands BPDB and BPDDB were synthesized in good yield by the Pd-catalyzed Sonogashira coupling reaction[29] between **1** or **2** and 4-bromopyridine in the presence of 6 mol % $PdCl_2(PPh_3)_2$ and 12 mol % CuI in *n*-propylamine (Scheme 1). The corner complexes, **8** and **9**, were prepared in refluxing isooctane solution containing $BrRe(CO)_5$ and excess ligand.[9b] Attempts to prepare *fac*-$BrRe(CO)_3(BPDB)_2$ or *fac*-$BrRe(CO)_3(BPDDB)_2$ in refluxing isooctane were unsuccessful. The crude products included a triangle and several unidentified products. This result is noteworthy and it will be discussed in more detail later. The self-assembly complexes **3**−**7** were prepared in essentially quantitative yield by reaction between $XRe(CO)_5$ (X = Cl or Br) and bridging ligands in refluxing toluene/THF mixture or neat benzene (Schemes 2 and 3).

The characterization of the molecular structures was achieved by a variety of analytical techniques including infrared spectroscopy, NMR spectroscopy, FAB^+ mass spectrometry, and elemental analysis. Infrared carbonyl stretching frequencies of these complexes exhibit tricarbonyl stretching patterns in the 1890−2030 cm^{-1} region that are typical for *fac*-$Re(LL)(CO)_3X$ complexes.[19] Elemental analysis confirms the 1:1 stoichiometry between Re(I) and bridging ligand. ^1H NMR spectroscopic data of **3** and **4** show simply two sets of doublets originating from α and β protons in the pyridine rings and this confirms the symmetric structures. As expected, both α- and β-pyridyl protons in **3** and **4** were shifted downfield relative to their free ligands, DPB and AZP, due to the dative bonding of the nitrogen lone pair to the Re(I) centers. FAB^+ mass spectral measurements yielded peaks at *m*/*z* 2002.4 (**3** − Cl^-) for **3** and *m*/*z* 1961.1 (**4** + H^+) for **4**. All these data support the square structures for **3** and **4**.

The roughly 120° bonding angle in BPET, however, prevents the formation of a square geometry. According to Stang's molecular library[4c] and from our molecular modeling results,[30] both trimeric and dimeric structures have comparable energies and are capable of forming through assembling of BPET and $ClRe(CO)_5$. Indeed, the ^1H NMR spectrum from the crude product exhibited two species in solution with a 4:1 ratio. Repeated recrystallization failed to separate these two species. Column chromatography on silica gel, first eluting with CH_2Cl_2, isolated a very small amount of yellow product. The ^1H NMR spectrum showed very complicated peak patterns which are not able to confirm the exact structure. The second deep yellow band was eluted with a 1:4 (v/v) ratio of THF/CH_2Cl_2. The ^1H NMR spectrum showed two downfield shifted clean doublets originating from pyridyl α and β protons and a singlet originating from the thiophene's protons. This compound corresponds to the major species observed in the ^1H NMR spectrum of the crude product. Elemental analysis established the 1:1 ratio between Re(I) and BPET for **5**.

FAB^+ mass spectral measurement for **5** confirmed its dimeric structure. Several reports from the literature have shown that the dimeric structure can be self-assembled from a labile *cis* transition metal component and a conformational flexible bridging ligand,[6c,e,31] while the formation of cyclic trimer (pseudohexagonal macrocycle) requires a more rigid bridging ligand and more precise coordinating direction toward the metal components.[32] The formation of a slightly more thermodynamically stable cyclic dimer over the corresponding cyclic trimer implies that, in this case, entropy effects play a more important role in the self-assembly process.

On the other hand, only unidentified oligomers were formed when refluxing BPDB and $BrRe(CO)_5$ in a 1:1 ratio of toluene/THF. Instead, **6** was prepared by refluxing BPDB and $BrRe(CO)_5$ in neat benzene with 90% isolated yield. The fact that **6** exhibits both light and thermal decomposition in THF solution may contribute to the inappropriateness of using THF as the solvent for synthesis of **6**. The incorporation of the long alkoxyl chains into the bridging ligand substantially increases the solubility of compound **6** in most moderately polar organic solvents. However, attempts to grow a single crystal of **6** from a variety of solvents or solvent combinations were still unsuccessful.

Interestingly, all spectroscopic data (NMR, IR) and elemental analysis for complex **6** are consistent with a square structure. However, the mass spectrum yielded a peak at 2494.2 ($M + H^+$), which corresponds to the triangular structure, and no peaks corresponding to square or higher order oligomers were found in the spectrum. The formation of a molecular triangle instead

(29) (a) Sonogashira, K.; Tohda, Y.; Hagihara, N. *Tetrahedron Lett.* **1975**, 4467. (b) Takahashi, S.; Kuroyama, Y.; Sonogashira, K.; Hagihara, N. *Synthesis* **1980**, 627. (c) Ziessel, R.; Suffert, J.; Youinou, M.-T. *J. Org. Chem.* **1996**, *61*, 6535. (d) Grosshenny, V.; Romero, F. M.; Ziessel, R. *J. Org. Chem.* **1997**, *62*, 1491.

(30) Based on the CAChe Work System 3.8, Oxford Molecular, Oxford, 1995. We realized that the energy minimization from molecular mechanics provides by no means the global energy minimized structure because the calculated structure highly depends on the local geometry from the starting model. However, the optimized geometry still can provide a good estimation of the molecular shape and size.

(31) (a) McMorran, D. A.; Steel, P. J. *Angew. Chem., Int. Ed. Engl.* **1998**, *37*, 3295. (b) Fan, J.; Whiteford, J. A.; Olenyuk, B.; Levin, M. D.; Stang, P. J.; Fleischer, E. B. *J. Am. Chem. Soc.* **1999**, *121*, 2741. (c) Schmitz, M.; Leininger, S.; Fan, J.; Arif, A. M.; Stang, P. J. *Organometallics* **1999**, *18*, 4817.

(32) Leininger, S.; Schmitz, M.; Stang, P. J. *Org. Lett.* **1999**, *1*, 1921.

Scheme 2

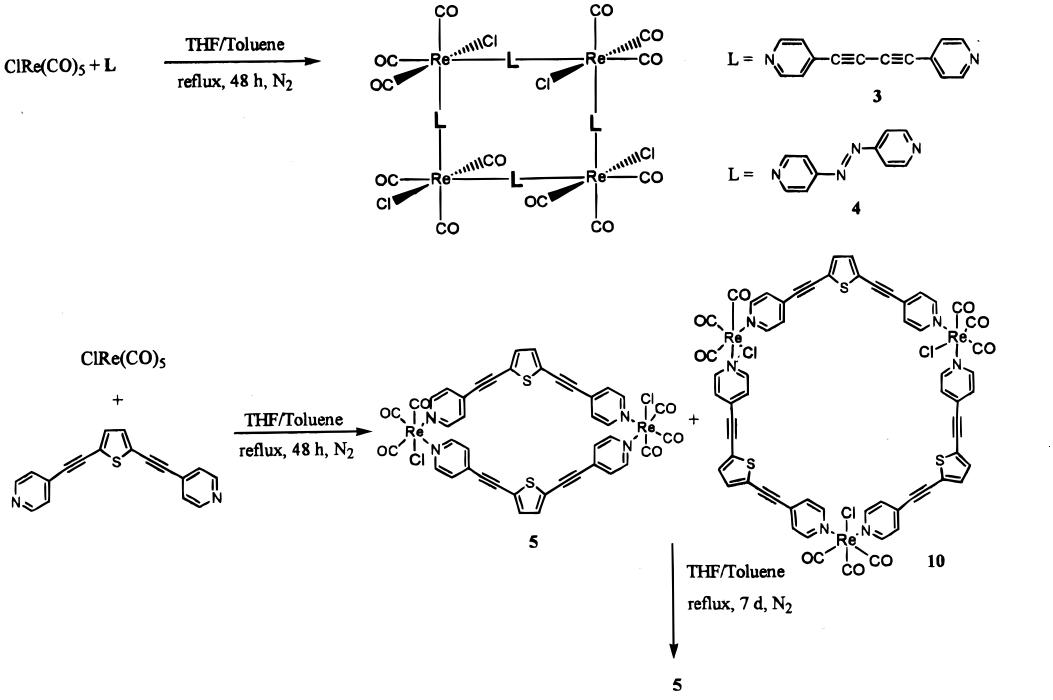

Scheme 3

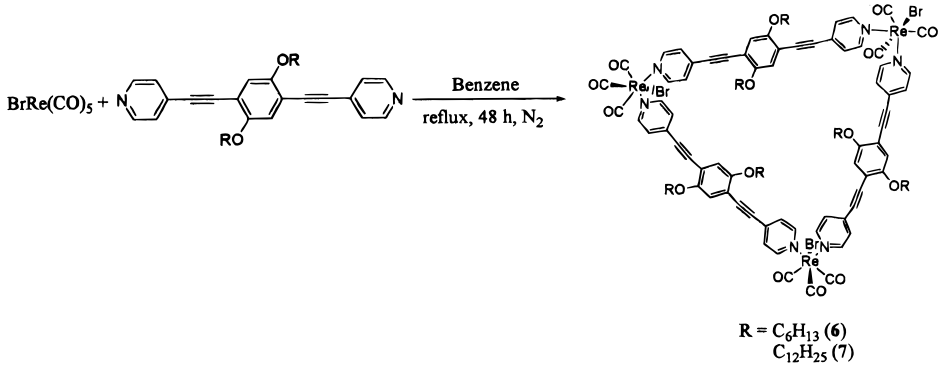

of a square indicates that the entropy term plays an important role in the self-assembly process, because the square structure is more stable in terms of enthalpy whereas entropy effects favor the triangular structure. The long hexoxyl groups in BPDB are believed to be responsible for this more favorable entropy contribution in the self-assembly process. Previously, Fujita et al. have observed the concentration-dependent equilibrium between the molecular square and triangle in the self-assembly process between (en)Pd(NO_3)$_2$ and DPB.[6d] Cotton et al. were also able to isolate the triangular or square complexes by simply changing the stoichiometry between the starting materials.[21h] However, we did not isolate any trace amount of the triangular structure from the assembly of $ClRe(CO)_5$ and DPB. The lack of a triangular structure is likely due to the poor solubility of **3** in a THF/toluene mixture and immediate precipitation from solution once the square is formed. In fact, Hupp and co-workers have isolated two different crystallographic forms, planar and folded, of [$ClRe(CO)_3$(μ-4,4′-bpy)]$_4$.[9e] The folded form is apparently more stable when the bridging ligand gets longer, as evident from molecular modeling. The larger BPDB ligand apparently makes the entropy effects more influential than the enthalpy effects. Also, the larger strain that exists in the triangular structure may be responsible for the increased thermal and photochemical decomposition of **6** in THF solution and the different photochemical behavior of the triangle **6** from the other square molecules, **3** and **4**.

Mechanism for Formation of the Self-Assembly Structures. Refluxing equimolar $XRe(CO)_5$ and bis-pyridyl ligand in a THF/toluene mixture is the protocol reaction condition for generating self-assembly square complexes.[9d] The labile solvento intermediate, $XRe(CO)_3(THF)_2$, forms first and then the thermodynamically most stable product precipitates from the solution.[9d] In this mechanism, the equilibrium-shifting precipitation of the square complexes plays an important role. The typically low solubility of square complexes (and other pre-square structures) in THF requires more soluble solvento complexes to keep the intermediates (dimers, trimers, etc.) in solution so that the thermodynamically structure-correcting processes can occur and the square complexes immediately precipitate from solution. There were either no cyclic structures formed or the products included many unidentified mixtures when we tried to prepare **3**−**5** in neat toluene or benzene as solvents, presumably due to the inability of toluene or benzene to form the solvento intermediates. It should also be noted that Hupp et al. observed no formation of square complexes in toluene and this further supports this mechanism.[9d]

On the other hand, we have found that triangle **6** does form in refluxing benzene (a noncoordinating solvent). The reason

Table 1. Redox Potentials[a]

compds	solvent	E_{ox} (ΔE_p, mV), V	E_{red} (ΔE_p, mV), V
$[ClRe(CO)_3(\mu\text{-DPB})]_4$	THF	*b*	−1.70 (i)
$[ClRe(CO)_3(\mu\text{-AZP})]_4$	DMF	1.32 (115)	−0.72 (80), −1.16 (135), −1.45 (i), −1.78 (85)
$[ClRe(CO)_3(\mu\text{-BPET})]_2$	CH_2Cl_2	1.03 (i), 1.29 (i)[c]	−1.66 (i)
$[BrRe(CO)_3(\mu\text{-BPDB})]_3$	DMF	1.06 (i)	−1.79 (i)
$[BrRe(CO)_3(\mu\text{-BPDDB})]_3$	DMF	1.07 (i)	−1.73 (i)
$BrRe(CO)_3(DPB)_2$	CH_2Cl_2	1.09 (i)	−1.69 (i), −1.97 (i)
$BrRe(CO)_3(AZP)_2$	DMF	1.18 (i)	−0.68 (84), −1.58 (i)
DPB	THF		>−2.00
AZP	DMF		−1.33 (90), −1.94 (i)
BPET	CH_2Cl_2	1.27 (i)[c]	>−2.00
BPDB	CH_2Cl_2		>−2.00
BPDDB	CH_2Cl_2		>−2.00

[a] Analyses were performed in 1 mM deoxygenated solutions containing 0.1 M TBAP; the scan rate is 250 mV/s. All potentials are in volts vs $[Fe(C_5H_5)_2]^{+/0}$ (0.11 V with a peak separation of 85 mV in DMF, 0.23 V with a peak separation of 130 mV in CH_2Cl_2, and 0.19 V with a peak separation of 118 mV in THF); (i) = irreversible process. [b] The oxidation potential is out of the solvent window. [c] Oxidation on thiophene.

is probably because of the better solubility of triangle **6** in comparison to simple Re(I) squares. Thus, the structure-correcting processes can still proceed in solution until the most thermodynamically stable product forms. To further test our hypothesis, complex **7** was prepared in the same procedure as triangle **6** by employing the bridging ligand, BPDDB, which contains dodecoxyl chains to increase the solubility in organic solvents. Again, the product formed in benzene was the self-assembly triangle without other oligomers. Besides, the failure to synthesize the corresponding corner complexes in refluxing isooctane even in the presence of a 10-fold excess of free BPDB or BPDDB also supports the presence of soluble kinetic products in hot isooctane, which can continue to self-assemble to the most thermodynamically stable product. Therefore, the more general mechanism of the self-assembly process between $XRe(CO)_5$ and bridging ligand can be described as follows: *The self-assembly process can proceed as long as the intermediates are soluble in the solvent or mixture of solvents so that the thermodynamically structure-error correcting process can continue until the most thermodynamically stable product forms*.

Electrochemical Properties. Redox potentials obtained from cyclic voltammograms of macrocycles **3**−**7** and their corner complexes and bridging ligands are presented in Table 1. All ligands showed reduction potentials higher than −2.0 V except AZP. These relatively low reduction potentials are ascribed to the addition of a pair of electrons to the lowest π^* orbital localized on the azo bond. Except for square **4**, all macrocyclic complexes exhibit one or two reduction waves corresponding to the reduction of bridging ligands and they vary depending on the properties of different ligands. These reduction potentials are much lower than those observed for the free ligands. The complexation of ligand to the metal usually stabilizes the π^* level in the ligand and lowers the energy of the π^* orbital.[33] In the case of complex **5**, two oxidation waves have been observed. The first oxidation potential is assigned to the formation of a cation radical localized on the thienyl moieties,[34] and the second oxidation potential is assigned to the oxidation localized on the metal centers. Due to the above-noted solubility limitation, cyclic voltammetry for square **3** can only be performed in THF solution and the oxidation potential is out of the THF window (~1.0 V). In general, the oxidation potentials for all macrocyclic compounds and their corresponding corners do not vary much and fall in the range between 1.03 and 1.32 V, which are

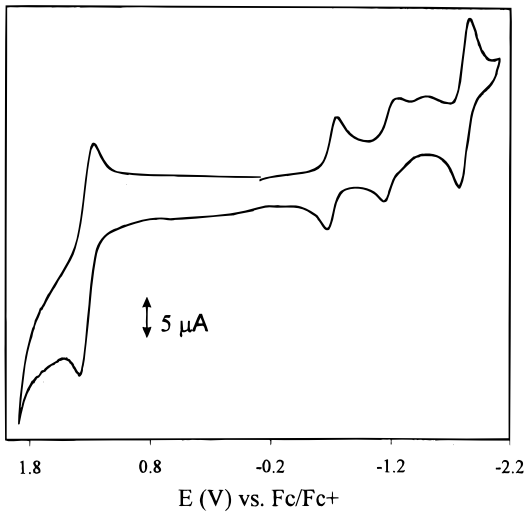

Figure 1. Cyclic voltammogram of square **4** in DMF/0.1 M Bu_4NClO_4 at a scan rate of 250 mV/s.

comparable to literature-reported values for a variety of polypyridyl rhenium tricarbonyl compounds.[33b,35] These results can be ascribed to the similar electronic environment that exists around the metal centers. Except for square **4**, all redox potentials of the macrocyclic compounds studied here are irreversible or only quasireversible at extremely high scan rates (>10 V/s). The metal-centered oxidation produces a labile 17-electron Re^{II} species[36] that undergoes facile CO substitution.[37]

Square **4** exhibits a reversible multielectron redox process (see Figure 1) that deserves further discussion. Due to its low-lying π^* LUMO of azo bond character, the AZP ligand is a stronger π acceptor compared to the other bridging ligands studied here and this property is also reflected in the higher oxidation potential (E_{ox}) for square **4**. Indeed, the E_{ox} for square **4** is 30 to 260 mV more positive than E_{ox} for the other macrocyclic compounds. The electrochemically quasireversible oxidation wave is indicative of a four-electron charge-transfer process and is assigned to a metal center oxidation ($Re^{1+/2+}$).[38,39] In contrast to the simple anodic electrochemical process, the cathodic electrochemical processes are more complicated. The first reversible reduction wave and second electrochemically

(33) (a) Zulu, M. M.; Lees, A. J. *Inorg. Chem.* **1988**, *27*, 1139. (b) Lin, J. T.; Sun, S.-S.; Wu, J. J.; Liaw, Y. C.; Lin, K. J. *J. Organomet. Chem.* **1996**, *517*, 217.

(34) (a) Thackeray, J. W.; White, H. S.; Wrighton, M. S. *J. Phys. Chem.* **1985**, *89*, 5133. (b) Zhu, S. S.; Swager, T. M. *J. Am. Chem. Soc.* **1997**, *119*, 12568. (c) Graf, D. D.; Mann, K. R. *Inorg. Chem.* **1997**, *36*, 150.

(35) Worl, L. A.; Duesing, R.; Chen, P.; Ciana, L. D.; Meyer, T. J. *J. Chem. Soc., Dalton Trans.* **1991**, 849.

(36) (a) Hershberger, J. W.; Klinger, R. J.; Kochi, J. K. *J. Am. Chem. Soc.* **1983**, *105*, 61. (b) Kochi, J. K. *J. Organomet. Chem.* **1986**, *300*, 139. (c) Tyler, D. R. *Prog. Inorg. Chem.* **1988**, *36*, 125.

(37) (a) Grob, R.; Kaim, W. *Inorg. Chem.* **1986**, *25*, 498. (b) Kaim, W.; Kramer, H. E. A.; Vogler, C.; Rieker, J. *J. Organomet. Chem.* **1989**, *367*, 107.

Table 2. Electronic Absorption and Emission Data at 293 K

compds	absorption spectra λ_{max}, nm (10^{-3}E, M^{-1} cm^{-1})	emission λ_{max}, nm	τ, ns	Φ_{em}
3[a]	256 (227), 298 (141), 322 (151), 360 (160)	635	39	8.5×10^{-4}
4[b]	272 (243), 391 (123)	*e*		
5[c]	383 (107), 422 (46.8)	*e*		
6[d]	329 (118), 406 (145)	499, 476	0.36	0.032
11[f]	338, 420	534	2.4	
7[d]	243 (86.4), 261 (71.6), 329 (113), 412 (142)	512, 470	0.37	0.012
12[g]	259, 277, 335, 414	536	2.9	
8[a]	250 (64.1), 287 (37.8), 301 (42.4), 320 (46.0), 342 (38.3)	600	110	0.011
9[b]	282 (56.8), 355 (22.9)	e		
DPB[a]	244 (18.9), 253 (17.8), 272 (8.1), 284 (11.9), 302 (15.2), 323 (13.2)	e		
AZP[c]	287 (19.9), 458 (0.24)	e		
BPET[c]	248 (14.6), 266 (13.2), 351 (47.7), 372 (sh, 36.2)	404, 384	0.26	0.26
BPDB[d]	308 (12.0), 318 (11.5), 377 (9.5)	450 (sh), 427	2.5	0.59
BPDDB[d]	308 (12.6), 318 (13.7), 340 (sh, 7.9), 388 (10.1)	446, 426	2.6	0.30

[a] THF solution, $\lambda_{ex} = 400$ nm. [b] DMF solution. [c] CH_2Cl_2 solution, $\lambda_{ex} = 360$ nm. [d] 1,2-DCE solution, $\lambda_{ex} = 360$ nm. [e] No detectable emission in room-temperature solution. [f] Photolysis of $[BrRe(CO)_3(\mu\text{-BPDB})]_3$ in 1,2-DCE at 313 nm after 20 h. [g] Photolysis of $[BrRe(CO)_3(\mu\text{-BPDDB})]_3$ in 1,2-DCE at 313 nm after 14 h.

quasireversible ($\Delta E_p = 135$ mV vs 85 mV for Fc/Fc^+ in DMF), but chemically reversible ($i_p^a/i_p^c = 1$) wave are assigned to the addition of four electrons successively to the lowest π^* orbital localized on the azo bond.[38] The last reversible two-electron reduction wave is assigned to the addition of two electrons to the lowest π^* orbital localized on the pyridyl rings. The third irreversible reduction wave is more uncertain in nature. We tentatively assigned this peak to the reduction of the metal center ($Re^{1+/0}$).[39] The capability of multiple charge storage and transfer within a single molecule is the prerequisite for molecules being used as energy conversion materials and/or electrocatalysts.[20] This multiple redox behavior in square **4** warrants further investigation of the charge-transfer capabilities and its potential applications.[40]

Photophysical Properties. Table 2 summarizes the photophysical data of complexes **3**−**7** as well as their corresponding corner complexes. The electronic absorption spectra of all the compounds exhibit two main features that are assigned as bridging-ligand-localized $\pi \rightarrow \pi^*$ and metal-to-bridging-ligand charge transfer (MLCT) transitions. In square **3**, the lowest-energy band is solely of MLCT character, while in compounds **4**−**7**, the $\pi \rightarrow \pi^*$ and MLCT bands are substantially overlapping. Square **4** exhibits an additional low-energy $n \rightarrow \pi^*$ transition that originates from the *trans*-AZP ligand which substantially overlaps with the MLCT band. Significantly, we find that the character of the lowest energy bands has a profound influence on the observed photophysical and photochemical properties.

Figure 2 compares the absorption spectra of square **3**, corner **8**, and free ligand DPB, in THF solution. It is very clear from the vibronic structure of the high-energy bands below 320 nm that these bands originate from DPB-localized $\pi \rightarrow \pi^*$ transitions. The lowest energy bands in square **3** and corner **8** are assigned to MLCT transitions. The MLCT band in square **3** red shifts 1385 cm^{-1} compared to that of the corner **8**. A similar red shift has also been observed from the protonated corner of *fac*-$ClRe(CO)_3(4,4'\text{-bpy})_2$ by Giordano and Wrighton.[41a] This result can be ascribed to either the fact that there is a more extended conjugation in square **3** than in corner **8** or the influence of the electrostatically stabilizing negative charge in the DPB π^* orbital by Re(I).[41]

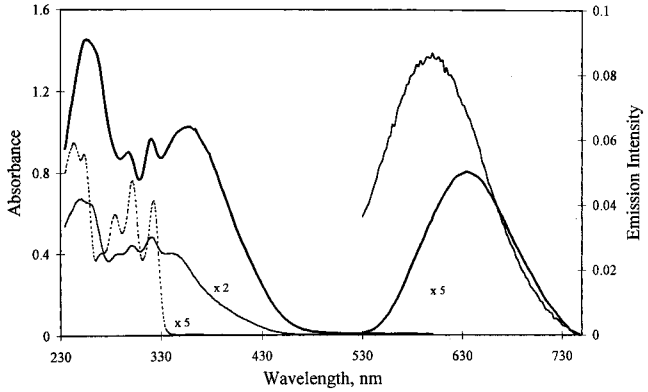

Figure 2. Electronic absorption and emission spectra of 7.5×10^{-6} M $[ClRe(CO)_3(\mu\text{-DPB})]_4$ (—), $ClRe(CO)_3(DPB)_2$ (−), and DPB (···) in THF at 293 K.

Square **3** exhibits luminescence at room temperature, which is independent of the excitation wavelength (340−400 nm), with an emission lifetime of 39 ns in THF solution. The wavelength-independent quantum yield and the good congruence between the absorption and excitation spectra of square **3** indicate that the internal conversion from higher excited states to the lowest ^{3}MLCT state is very efficient and that luminescence originates solely from the lowest ^{3}MLCT state. The assignment of the lowest emitting level as MLCT in character is based on the position and shape of the emission band and the emission lifetime which are consistent with those previously reported for similar complexes assigned as MLCT emitters.[41−43] As observed in the absorption spectra, the emission maxima of square **3** shifts to lower energy compared to the emission maxima of its corner **8**. The emission lifetime of square **3** is shorter than its corner **8**; this is attributed to an enhanced nonradiative decay rate for

(38) (a) Flanagan, J. B.; Margel, S.; Bard, A. J.; Anson, F. C. *J. Am. Chem. Soc.* **1978**, *100*, 4248. (b) Stor, G. J.; Hartl, F.; van Outersterp, J. W. M.; Stufkens, D. J. *Organometallics* **1995**, *14*, 1115. (c) Kelso, L. S.; Reitsma, D. A.; Keene, F. R. *Inorg. Chem.* **1996**, *35*, 5144. (d) Otsuki, J.; Tsujino, M.; Iizaki, T.; Araki, K.; Seno, M.; Takatera, K.; Watanabe, T. *J. Am. Chem. Soc.* **1997**, *119*, 7895.

(39) (a) Caspar, J. V.; Sullivan, B. P.; Meyer, T. J. *Inorg. Chem.* **1984**, *23*, 2101. (b) Sullivan, B. P.; Bolinger, C. M.; Conrad, D.; Vining, W. J.; Meyer, T. J. *J. Chem. Soc., Chem. Commun.* **1985**, 1414. (c) Moya, S. A.; Guerrero, J.; Pastene, R.; Schmidt, R.; Sariego, R.; Sartori, R.; Sanz-Aparocop, J.; Fomseca, I.; Martinez-Ripoll, M. *Inorg. Chem.* **1994**, *33*, 2341.

(40) Sun, S.-S.; Lees, A. J. Work in progress.

(41) (a) Giordano, P. J.; Wrighton, M. S. *J. Am. Chem. Soc.* **1979**, *101*, 2888. (b) Callahan, R. W.; Brown, G. M.; Meyer, T. J. *Inorg. Chem.* **1980**, *19*, 2797. (c) Sun, S.-S.; Robson, E.; Dunwoody, N.; Silva, A. S.; Brinn, I. M.; Lees, A. J. *Chem. Commun.* **2000**, 201.

(42) Caspar, J. V.; Meyer, T. J. *J. Phys. Chem.* **1983**, *87*, 952.

(43) Baba, A. I.; Shaw, J. R.; Simon, J. A.; Thummel, R. P.; Schmehl, R. H. *Coord. Chem. Rev.* **1998**, *171*, 43.

Scheme 4

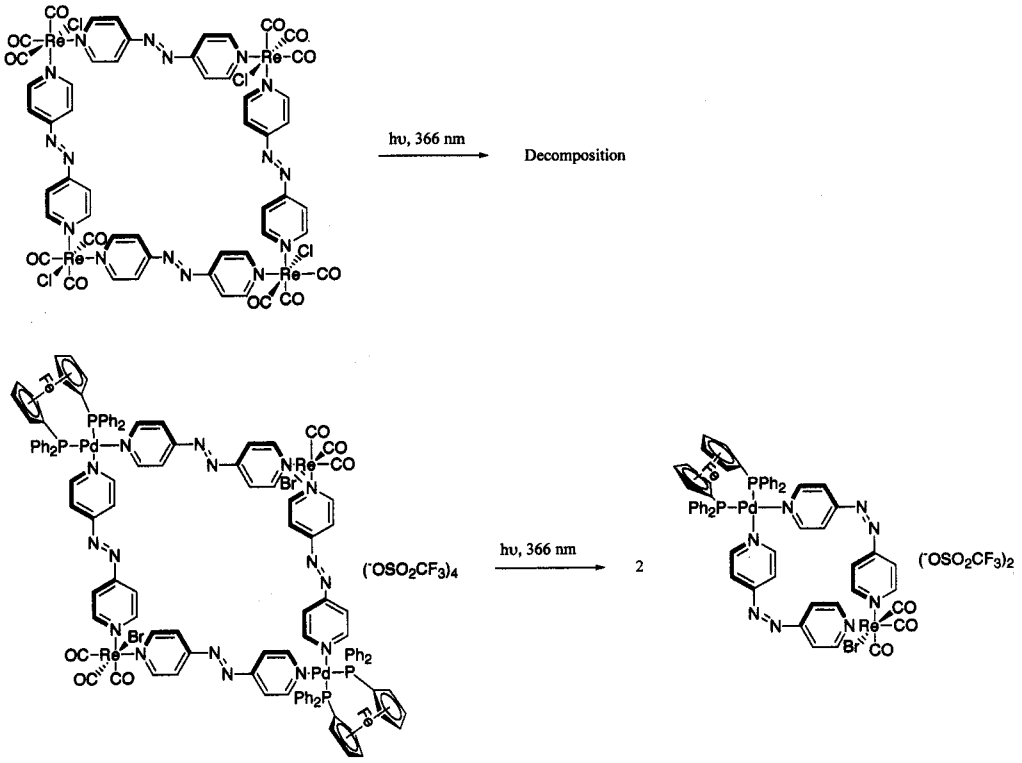

square **3** due to the lower energy of the excited state with a more effective vibronic overlap.[41,42]

In contrast, neither square **4** nor its corner **9** have any detectable luminescence at room temperature under the same experimental conditions. This is attributed to effective intramolecular energy transfer from the initially formed ^{1,3}MLCT excited states to the lowest nonemitting n → π^* state.[44] It is well-known that compounds containing the azo group exist in both *cis* and *trans* isomers and they are readily susceptible to photoisomerization.[45] Indeed, photolysis of corner **9** at 366 nm resulted in *trans*-AZP to *cis*-AZP isomerization. However, photolysis of **4** at 366 or 313 nm resulted in slow decomposition and there was no sign of isomerization. This result is in contrast to the result obtained from photolysis studies of cyclobis[(dppf)Pd(μ-AZP)$_2$-Re(CO)$_3$Br](OTf)$_4$ (dppf is 1,1′-diphenylphosphinoferrocene and OTf is $CF_3SO_3^-$) at 366 nm; here the isomerization of the bridging ligand induced the conversion from the tetranuclear species to the dinuclear species (see Scheme 4).[46] These observations are associated with the different lability of Pd(II) and Re(I) in solution. The *trans*−*cis* isomerization process generates a large strain on the square structure and causes the breaking of metal−nitrogen bonds. At room temperature, the more labile Pd(II) metal center can more readily undergo the *trans*−*cis* conformational change and form the dimeric structure, while the more inert Re(I) is unable to recombine the Re−N bonds and decomposition occurs immediately after ligand isomerization.

The lone pairs on the azo group in the AZP ligand are susceptible for protonation in acidic environment.[47] UV−visible spectrophotometric titration of square **4** by HCl was performed in DMSO solution. The MLCT band that is centered at 386 nm blue shiftes with increasing H^+ equivalent and reaches the final spectrum with a band maxima at 362 nm after the addition of 8 equiv of H^+ (see Supporting Information). This result cannot be explained by a simple protonation reaction on the central azo groups. If this is the case, the electron-withdrawing characteristic of protonated azo group will lower the π^* level and a red shift should be observed.

In pH 7 aqueous solution, 4,4′-azopyridine is very easily reduced to 1,2-bis(4-pyridyl)hydrazine (BPH) with $E°$ near 0 V vs SCE.[48] In acidic DMSO solution, the reduction process is expected to be even easier. Consequently, we suggest that the spectral changes are accompanied by a proton-induced reduction on the AZP ligand (see Scheme 5).[25] The electron-donating amine group on BPH has a higher π^* level than the azo group on AZP and, thus, the blue shift in the absorption spectra is observed upon H^+ titration.

The absorption spectrum of the cyclic dimer **5** features a broad band centered at 383 nm and a shoulder at 422 nm. The low-energy shoulder is assigned to be MLCT in character and the band at 383 nm is assigned to a ligand localized $\pi \rightarrow \pi^*$ transition. In contrast to its free ligand (BPET), which exhibited strong fluorescence in room-temperature CH_2Cl_2 solution, there is no luminescence detected from **5** under the same conditions. The lack of emission is also attributed to the efficient vibrational relaxation on the basis of the energy gap law.[42]

The detailed photophysical data of **6** and **7** are summarized in Table 2. In general, the photophysical properties of triangles **6** and **7** are very similar. The following discussion will mainly focus on triangle **6**, but will point out any notable differences in the physical properties of **7**. The absorption spectrum of **6** differs significantly in comparison to its corresponding free bridging ligand, BPDB. The spectrum of **6** exhibits two broad bands and both bands are red-shifted compared to the absorption bands of BPDB. The intensity ratio of the lower-energy band

(44) Yam, V. W.-W.; Lau, V. C.-Y.; Wu, L.-X. *J. Chem. Soc., Dalton Trans.* **1998**, 1461.

(45) Balzani, V.; Scandola, F. *Supramolecular Photochemistry*; Ellis Horwood: Chihester, U.K., 1991.

(46) Sun, S.-S.; Lees, A. J. Manuscript in preparation.

(47) Gerson, F.; Heilbronner, E. *Helv. Chim. Acta* **1962**, *45*, 51.

(48) Haladjian, J.; Pilard, R.; Bianco, P.; Asso, L.; Galy, J. P.; Vidal, R. *Electrochim. Acta* **1985**, *30*, 695.

Scheme 5

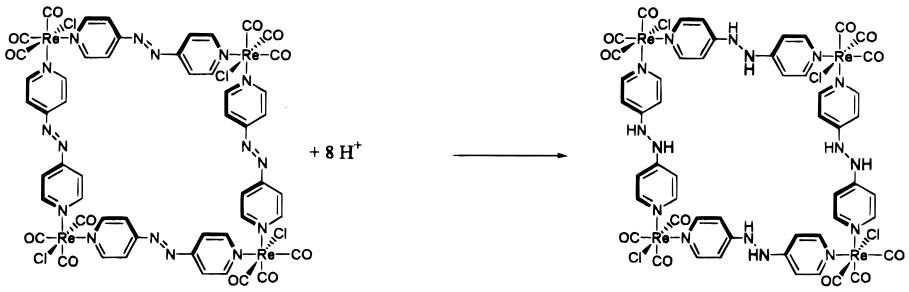

vs the higher-energy band is also larger in **6** than the corresponding ratio in BPDB. The lowest-energy band is assigned to a mixture of MLCT and $\pi \rightarrow \pi^*$ excited states. The room-temperature emission spectrum of **6** in 1,2-DCE exhibits structured features with maxima at 499 and 476 nm. It should be noted that the luminescence is not dependent on the excitation wavelength in the 340−400 nm range and that there is a single-exponential decay from these two bands. The low-temperature (77 K) emission spectrum of **6** in 2-methyltetrahydrofuran (MeTHF) displays more distinct structure with bands at 463, 488, 520, and 549 nm (1188 cm^{-1} average spacing). These observations illustrate that the dual emission bands are actually vibronic structure from the $\pi-\pi^*$ excited state. The very small blue shift on going from the solution to a rigid glass also supports the assignment of the emission from a ligand-based $\pi \rightarrow \pi^*$ excited state.[19a,49]

Careful scrutiny of the photophysical data of triangle **6** and its free ligand, BPDB, reveals several interesting points. The extremely short lifetime and relatively high-energy emission from **6** indicate that the emission is apparently BPDB-localized $^1\pi-\pi^*$ fluorescence. Fluorescence from a $^1\pi-\pi^*$ state is typically not observed in transition metal complexes.[19a] However, the fast radiative decay rate ($k_r \sim 10^8\ s^{-1}$) from the $^1\pi-\pi^*$ excited state localized on BPDB is apparently still able to compete with other internal conversion processes. In addition, BPDB exhibits a longer lifetime than **6** and the quantum yield of BPDB is almost 20 times larger than that in **6**. On this basis, it can be concluded that the $Re(CO)_3Br$ moieties in **6** act as energy quenchers. Consequently, the relatively low fluorescence quantum yield and short lifetime in room-temperature solution are due to the intramolecular energy transfer from the $^1\pi-\pi^*$ state to the ^{3}MLCT or $^3\pi-\pi^*$ states.[50] Considering the large spin−orbital coupling exerted from Re(I) atoms,[19a] it is unusual that there is no phosphorescence observed from either the ^{3}MLCT or $^3\pi-\pi^*$ excited states in triangle **6**. If we treat complex **6** as a cyclic trimer, the folding motions of the hexoxyl chains in **6** are believed to be responsible for the rapid vibrational relaxation from the ^{3}MLCT excited state. This is further supported by the higher quantum yield of BPDB and its corresponding triangle in comparison to BPDDB and its corresponding triangle. In fact, in addition to the vibronic structures observed at high-energy positions, a very weak emission centered at 602 nm with a lifetime 163 μs was also observed in a 77 K glass (see Figure 3). This structureless band is too low in energy to be one of the vibronic features from the $\pi-\pi^*$ excited state. Thus, it is reasonable to assign this band as a ^{3}MLCT transition on the basis of the absence of vibrational structure, although some incorporation of $^3\pi-\pi^*$ character cannot be completely ruled out.[43]

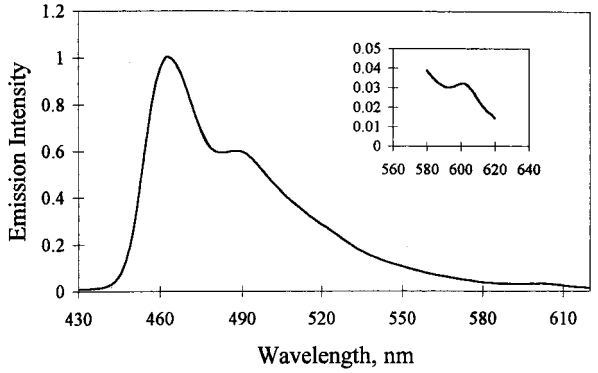

Figure 3. Emission spectrum of $[BrRe(CO)_3(\mu\text{-BPDB})]_3$ in 77 K 2-MeTHF glass. The inset shows the lowest-energy band.

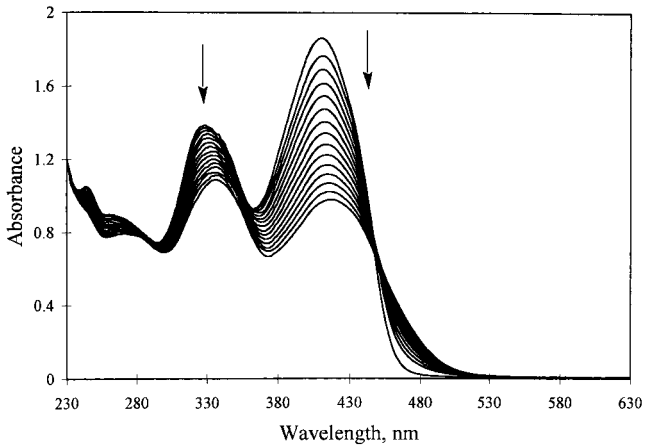

Figure 4. Absorption spectra of $[BrRe(CO)_3(\mu\text{-BPDB})]_3$ in 1,2-DCE at 293 K as a function of photolysis time ($\lambda_{ex} = 313$ nm). $t = 0$, 1, 2, 3, 4, 5, 6, 7, 8, 9, 10, 11, 12, 13, 14 h.

Photochemical Properties. The highly strained triangular structures of **6** and **7** suggest that the thermodynamical stability of **6** and **7** may be altered by external stimuli such as light. Photolysis into the $\pi-\pi^*$ transition at 313 nm resulted in both absorption bands slowly decreasing and red shifting. The emissions are also red-shifted upon photolysis. The two absorption bands are moved from 329 and 406 nm to 338 and 420 nm, respectively. The relative intensity of these two absorption bands also changes during photolysis. Figures 4 and 5 present the progression of absorption spectra of **6** and the corresponding luminescence spectra in deoxygenated 1,2-DCE solution as a function of photolysis time. The appearance of an isosbestic point at 436 nm in the absorption data indicates a clean photochemical conversion from triangle **6** to a final product. The luminescence spectrum is also red-shifted with bands at 499 and 476 nm moving to 534 nm. There is no further shifting

(49) Juris, A.; Campagna, S.; Bidd, I.; Lehn, J.-M.; Ziessel, R. *Inorg. Chem.* **1988**, *27*, 4007.

(50) (a) Ley, K. D.; Li, Y.; Johnson, J. V.; Powell, D. H.; Schanze, K. S. *Chem. Commun.* **1999**, 1749. (b) Ley, K. D.; Schanze, K. S. *Coord. Chem. Rev.* **1998**, *171*, 287. (c) Ley, K. D.; Whittle, C. E.; Bartberger, M. D.; Schanze, K. S. *J. Am. Chem. Soc.* **1997**, *119*, 3423.

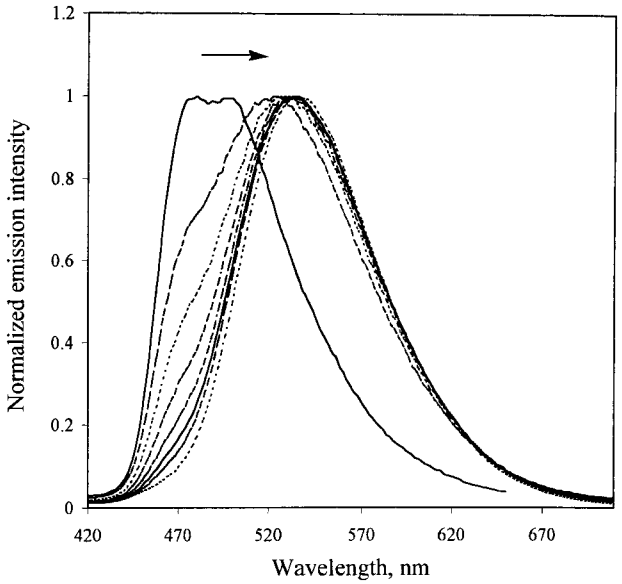

Figure 5. Normalized emission spectra of $[BrRe(CO)_3(\mu\text{-BPDB})]_3$ in 1,2-DCE at 293 K as a function of photolysis time ($\lambda_{ex} = 313$ nm). $t = 0, 1, 2, 3, 4, 5, 6, 14$ h.

Chart 2

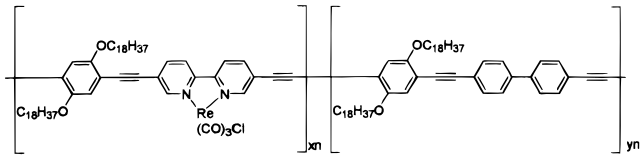

of the emission spectrum after 14 h of photolysis. Similar absorption spectral changes with an isosbestic point at 448 nm are also observed in triangle **7** when photolyzed at 313 nm. The lifetime measured is 2.4 ns for the photolysis product from **6** after 20 h of irradiation and 2.9 ns for the photolysis product from **7** after 14 h of photolysis, which are both very close to the lifetimes of their corresponding free ligands. The infrared spectrum in 1,2-DCE for the photolysis product from **6** after 14 h of irradiation exhibits υ_{CO} bands at 2025, 1925, and 1892 cm^{-1} compared to 2025, 1924, and 1892 cm^{-1} before photolysis. Also, the infrared spectrum in 1,2-DCE for the photolysis product from **7** after 6 h of irradiation exhibits υ_{CO} bands at 2025, 1928, and 1892 cm^{-1} compared to 2025, 1925, and 1892 cm^{-1} before photolysis. As expected, the infrared spectra do not show too much difference before and after photolysis because the local environments around Re(I) are quite similar in these triangular and polymeric structures.

The features of the final absorption spectrum after photolysis closely resemble the absorption spectra of $(diimine)ClRe(CO)_3$ chromophores containing polymeric systems studied by Schanze et al. (Chart 2).[50] The GPC data showed that the molecular weights (M_n) of photolysis products from **6** and **7** are 12300 (polydispersity = 3.6) and 15600 (polydispersity = 4.7), respectively. In light of all the above results, we tentatively assigned the photolyzed products from **6** or **7** to zigzag polymeric structures (see Scheme 6). The red shifts in the absorption and emission spectra are believed to occur because the breaking of the triangle releases the steric strain associated with the structure and this increases the conjugation of the aromatic system.

Host−Guest Interactions. Luminescent compounds with internal cavities have been shown to have potential applications as chemosensory devices in recent years.[51] Many macrocyclic complexes have been studied for their molecular recognition capabilities toward small aromatic molecules,[6a−c,7a,b,52] inorganic anions,[9a,18] or porphyrin molecules,[9c−g] based on their different cavity sizes and intermolecular forces such as hydrogen bonding and hydrophobic or electrostatic interactions. Hupp et al. have elegantly demonstrated that different sized rhenium tricarbonyl based square complexes can effectively select different sized guest molecules by electrochemical transport experiments.[9e−g,52] In fact, these square complexes are packed with infinite channels in their solid states.[9b,e,53] Such properties render these macrocyclic molecules potential hosts for certain aromatic molecules in the solid state as well as in solution.

Chart 3

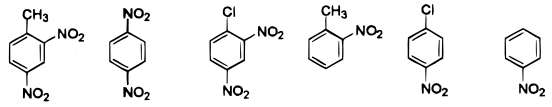

	DNT	DNB	CDNB	NT	ClNB	NB
rel. VP[54]	6	1	3	7700	1000	10000
E_{red} (V)[55]	-1.0	-0.7	-0.8	-1.28	-1.1	-1.15

Host−Guest Interactions Studied by ^{1}H NMR. Several aromatic compounds have been studied for their potential chemistry in solution. For all the aromatic compounds tested here which include toluene, *p*-methoxybenzene, 1,3,5-trimethoxybenzene, naphthalene, and several nitro-substituted aromatic compounds, none of them showed any significant binding interactions with triangles **6** and **7** because the peak shifts in the ^{1}H NMR spectral peaks are all smaller than 0.01 ppm. These results are not too unexpected as the energy minimized molecular structures for triangles **6** and **7** derived from CAChe MM2 molecular modeling showed very limited internal voids due to the long alkoxyl groups penetrating through the voids (see Supporting Information).

Host−Guest Interactions Studied by Luminescence. Whereas typical aromatic compounds encapsulated inside the metallo-cyclophane structures are not expected to result in significant changes in the luminescence properties, nitro-substituted aromatic compounds may be capable of serving as electron acceptors from the excited state and, thus, able to quench the luminescence. A series of nitro-substituted aromatic compounds (see Chart 3) have been used to test for quenching effects. In THF solution, the luminescence of both square **3** and its corner **8** is effectively quenched by these nitro-substituted aromatic compounds with quenching constants ranged from 4.94×10^8 to 9.12×10^9 M^{-1} s^{-1}.[56]

In solid films, the luminescence spectral bands from both square **3** and corner **8** are blue shifted compared to their corresponding luminescence in solution. This phenomenon is

(51) (a) *Chemosensors of Ion and Molecule Recognition*; Desvergne, J. P., Czarnik, A. W., Eds.; Kluwer Academic Publishers: Boston, 1997. (b) de Silva, A. P.; Gunaratne, H. Q.; Gunnlaugsson, N. T.; Huxley, A. J. M.; McCoy, C. P.; Rademacher, J. T.; Rice, T. E. *Chem. Rev.* **1997**, *97*, 1515 and references therein. (c) Yang, J.-S.; Swager, T. M. *J. Am. Chem. Soc.* **1998**, *120*, 5321, 11864.

(52) Keefe, M. H.; Slone, R. V.; Hupp, J. T.; Czaplewski, K. F.; Snurr, R. Q.; Stern, C. L. *Langmuir*, **2000**, *16*, 3964.

(53) Bélanger, S.; Hupp, J. T.; Stern, C. L. *Acta Crystallogr.* **1998**, *C54*, 1596.

(54) *Handbook of Physical Properties of Organic Chemicals*; Howard, P. H., Meylan, W. M., Eds.; CRC Press: Boca Raton, FL, 1997.

(55) *Handbook Series in Organic Electrochemistry*; Meites, L., et al., Eds.; CRC Press: Boca Raton, FL, 1978; Vol. 1.

(56) See Supporting Information for their quenching constants derived from Stern−Volmer analysis.

Scheme 6

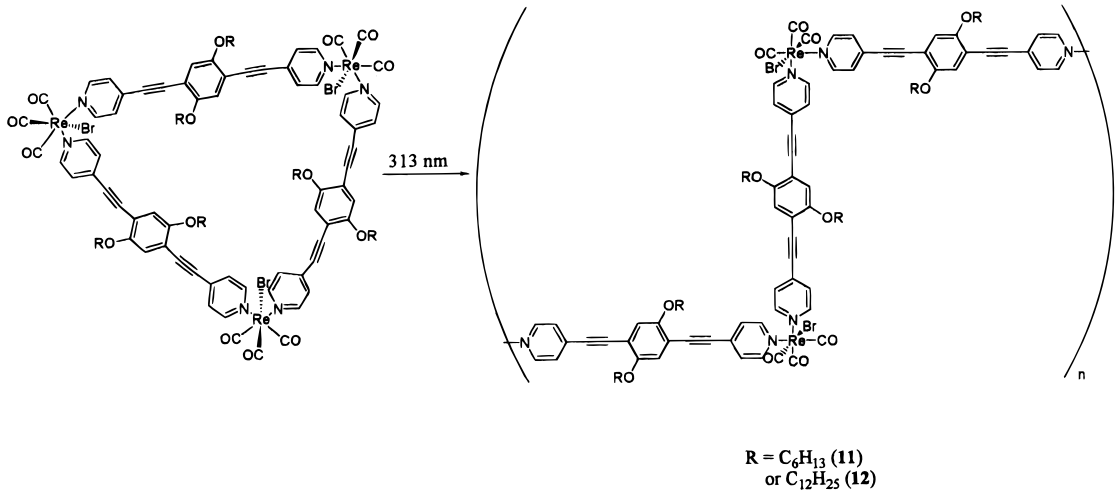

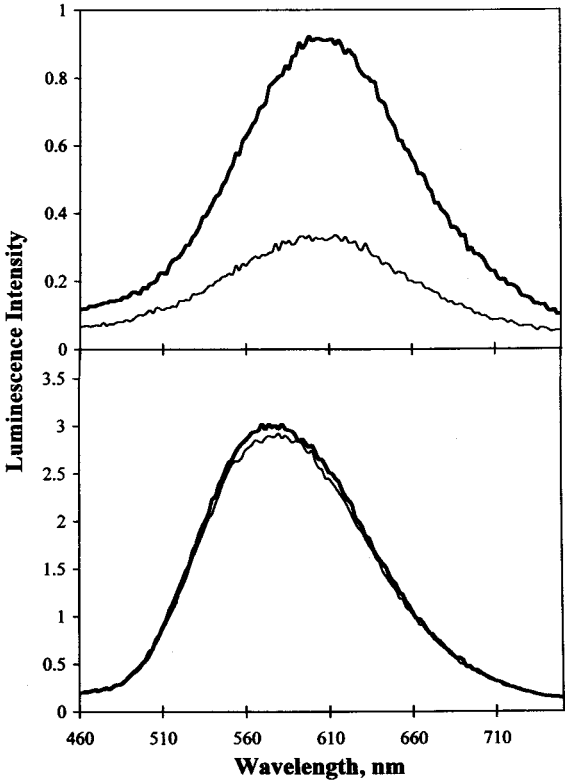

Figure 6. Luminescence response of films of square **3** (top) and corner **8** (bottom) upon exposure to DNT vapor for 180 s. The thick and thin lines represent the luminescence before and after exposure to DNT vapor, respectively.

recognized as a luminescence rigidochromic effect.[57] In solution, the quenching constants are mainly determined by the electron-transfer rate from **3** or **8** to the quenchers and are, thus, dependent on the free energy change ($\Delta G°$). For an oxidative electron-transfer reaction, the $\Delta G°$ can be approximated according to $\Delta G° = E_{ox} - E_{0-0} - E_{red}$, where E_{ox}, E_{0-0}, and E_{red} are oxidation potentials of **3** or **8**, the lowest triplet 0−0 excited-state energy of **3** or **8**, and the reduction potentials of the quenchers, respectively. Given the higher E_{0-0} of corner **8** than E_{0-0} of square **3**, the quenching constants in THF solution for corner **8** are generally larger than those for square **3**.[56]

(57) (a) Wrighton, M. S.; Morse, D. L. *J. Am. Chem. Soc.* **1974**, *96*, 998. (b) Lees, A. J. *Comm. Inorg. Chem.* **1995**, *17*, 319 and references therein.

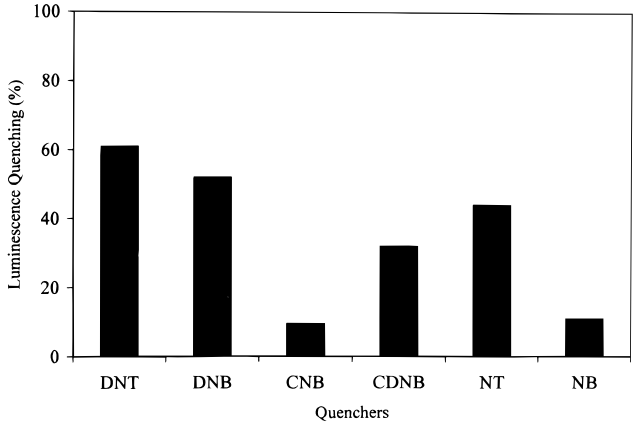

Figure 7. The percent quenching of the luminescence of square **3** film after exposure to vapor of different quenchers at 180 s.

However, in these solid films, more factors need to be considered to rationalize the luminescence quenching, namely, $\Delta G°$, vapor pressure (VP) of the quenchers, and the binding constant (K_b). Figure 6 compares the luminescence response of films of square **3** and corner **8** to the vapor of 2,3-dinitrotoluene (DNT) at 180 s. Clearly, only square **3** displays significant luminescence quenching after exposure to the vapor of DNT in the solid film. The main factor that results in the substantially different quenching effect between the square **3** and corner **8** in the solid films is the difference in binding strength toward the quencher. The quenching effect appearing in the film of square **3** is apparently due to the porosity that exists in the film, which provides cavities for binding the quencher molecules.[9e,52] Figure 7 summarizes the quenching effects by different quenchers. In general, higher vapor pressure from the quenchers that can bring greater numbers of binding molecules toward the square and more nitro groups in the quenchers that are able to provide a greater electronic interaction between the film and the quenchers will result in larger quenching effects.[51c]

Conclusion

We have demonstrated here that different geometric macrocyclic supramolecules can be prepared, in a predictable way, by assembling suitable polypyridyl bridging ligands and *fac*-$XRe(CO)_3$ corners. The electrochemical, photophysical, and photochemical properties of these macrocyclic supramolecules are highly dependent on the nature of the bridging ligand. A more generalized mechanism for the self-assembly process is

proposed which involves intermediates which are soluble in solution so that the structure-error correcting processes can proceed until the most thermodynamically stable product appears.

A series of guest inclusion studies have revealed that these macrocyclic compounds are efficient hosts for nitro-substituted aromatic molecules. The incorporation of luminescent chromophores into the host molecules provides a more sensitive spectroscopic detection technique than the conventional NMR method for monitoring the host−guest interactions. Through current binding studies in solution as well as in the solid state, we have demonstrated that these macrocyclic compounds can be effectively used in sensor applications by detecting the luminescence.

Acknowledgment. We are grateful to the Division of Chemical Science, Office of Basic Energy Sciences, Office of Energy Research, U.S. Department of Energy (Grant DE-FG02-89ER14039), for support of this research. We also thank Prof. Omowunmi A. Sadik for access to electrochemical equipment and Prof. Jiann T. Lin at the Institute of Chemistry, Academia Sinica at Taipei, Taiwan for help in obtaining mass spectra of complexes **3** and **6**.

Supporting Information Available: A table listing solution quenching constants of square **3** and corner **8** obtained from Stern−Volmer analysis with different nitro-substituted aromatic compounds, a figure showing the spectrophotometric titration of square **4** by HCl in DMSO solution, and a figure showing the space-filling structures derived from CAChe MM2 molecular modeling for macrocyclic compounds **3**−**7** (PDF). This material is available free of charge via the Internet at http://pubs.acs.org.

JA001677P